Using Laser-Induced Rydberg Spectroscopy diagnostic for direct measurements of the local electric field in the edge region of NSTX/NSTX-U: Modeling

L. Reymond, A. Diallo, and V. Vekselman

Citation: Review of Scientific Instruments **89**, 10C106 (2018); doi: 10.1063/1.5038877
View online: https://doi.org/10.1063/1.5038877
View Table of Contents: http://aip.scitation.org/toc/rsi/89/10
Published by the American Institute of Physics

Using Laser-Induced Rydberg Spectroscopy diagnostic for direct measurements of the local electric field in the edge region of NSTX/NSTX-U: Modeling

L. Reymond,[1,a)] A. Diallo,[2,b)] and V. Vekselman[2]
[1]*Swiss Plasma Center, Ecole Polytechnique Fédérale de Lausanne (EPFL), Lausanne, Switzerland*
[2]*Princeton Plasma Physics Laboratory, Princeton University, Princeton, New Jersey 08540, USA*

(Presented 17 April 2018; received 6 May 2018; accepted 14 July 2018;
published online 6 August 2018)

We discuss a novel diagnostic allowing direct measurements of the local electric field in the edge region of NSTX/NSTX-U. This laser based diagnostic's principle consists of depleting the naturally populated $n = 3$ level to a Rydberg state—sensitive to electric fields—that will result in a suppression of part of the D_α emission. We refer to this approach as Laser-Induced Rydberg Spectroscopy. It is shown that the local electric field can be measured through the Stark induced resonances observed as dips in the D_α emission. Using forward-modeling of simulated absorption spectra, we show precisions reaching ± 2 kV m^{-1} in regions with a local electric field of 15 kV m^{-1}. *Published by AIP Publishing.*
https://doi.org/10.1063/1.5038877

I. INTRODUCTION

The electric field ($\mathcal{E}$) plays a crucial role in the edge dynamics, the overall plasma confinement, and therefore fusion performance. The electric field profile is among the plasma parameters that are most difficult to measure and hence has been largely neglected for many years. Radial electric fields in magnetically confined plasma have been recently characterized by various diagnostic techniques,[1–3] but none of them provides a direct and local measurement. Most of the radial electric field ($\mathcal{E}_r$) measurements in current fusion devices rely on the radial force balance. One direct approach of measuring the electric field is the heavy-ion beam probe (HIBP).[4,5] This approach provides direct but *nonlocal* measurements of $\mathcal{E}_r$ and can be quite difficult to implement at the edge of fusion devices. Extraction of the radial electric field component from the motional Stark effect (MSE) measurements requires complex geometry and features low spatial resolution and sensitivity.[6] The topic of the electric field in toroidal devices (e.g., stellarators and tokamaks) has been reviewed by Ida.[7] In addition, Donné[8] discussed the need to diagnose the electric field in order to actively control the internal edge transport barriers in tokamaks.

Below, we describe the fluorescence dip approach using Rydberg's level to sense the electric field in the edge of magnetically confined plasmas. We refer to this approach as Laser-Induced Rydberg Spectroscopy (LIRyS) for the remainder of the paper. The proposed laser-based approach provides direct measurements of the electric field. In this paper, we describe the forward modeling of LIRyS diagnostic in NSTX (and NSTX-U).

Note: Paper published as part of the Proceedings of the 22nd Topical Conference on High-Temperature Plasma Diagnostics, San Diego, California, April 2018.
[a)]Electronic mail: loic.reymond@alumni.epfl.ch
[b)]Electronic mail: adiallo@pppl.gov

II. DESCRIPTION OF THE LIRyS APPROACH

A. Elements of theory

The proposed diagnostic is based on the *Stark effect* that is responsible for the splitting of the energy levels (E) in plasmas. For hydrogen-like atoms—such as deuterium D—with atomic number Z, the energy levels are described according to the following equation:[9,10]

$$E = -A_0\left(\frac{n}{Z}\right)^{-2} + \mathcal{E}A_1\left(\frac{n}{Z}\right)(n_2 - n_1) - \mathcal{E}^2A_2\left(\frac{n}{Z}\right)^4\left(17n^2 - 3(n_2 - n_1)^2 - 9m_\ell^2 + 19\right) + \mathcal{O}\left(\mathcal{E}^3\right), \quad (1)$$

where $\mathcal{E}$ (kV m^{-1}) is the electric field's amplitude, $n_1 = 0, \ldots, n-1$ and $n_2 = 0, \ldots, n-1$ are the parabolic quantum numbers[11] that appear also in the magnetic quantum number $m_\ell = n - 1 - n_1 - n_2$. Expressions of the coefficients A_0, A_1, and A_2 are listed in Table I.

For a given transition, this splitting is unique and is determined by the magnitude of the external electric field $\mathcal{E}$ applied to the atom. The energy splitting for a given $\mathcal{E}$ is larger for highly excited Rydberg states, motivating the extensive use of Rydberg atoms in various diagnostics. In addition, the presence of neutral and charged particles in plasma disturbs energy levels; commonly observed as a broadening of the radiative transition between the pair of energy levels. In the edge region of NSTX/NSTX-U, the combination of the splitting and broadening of transition lines is continuously monitored through the emission of D_α radiation (transition $n = 3 \rightarrow 2$). To probe the electric field, we induce a dip in D_α emission by depopulating the $n = 3$ level toward a selected Rydberg state. The observed dip can be linked to a value of the local electric field.[12,13] The scheme is illustrated in Fig. 1 where the frequency-tunable probe laser (4 pm linewidth, 20 ns pulse duration) is used

TABLE I. Stark coefficients, up to the second order. $\mu = 0.999\,728\ m_e$ is the deuterium reduced mass.

A_0	$\frac{\mu}{2}\frac{e^4}{\hbar^2}(4\pi\varepsilon_0)^{-2}$	91.152 nm
A_1	$\frac{3}{2\mu}\frac{\hbar^2}{e}(4\pi\varepsilon_0)$	1.5616×10^{10} nm (kV/m)$^{-1}$
A_2	$\frac{1}{2^4\mu^3}\frac{\hbar^6}{e^6}(4\pi\varepsilon_0)^4$	1.9261×10^{20} nm (kV/m)$^{-2}$

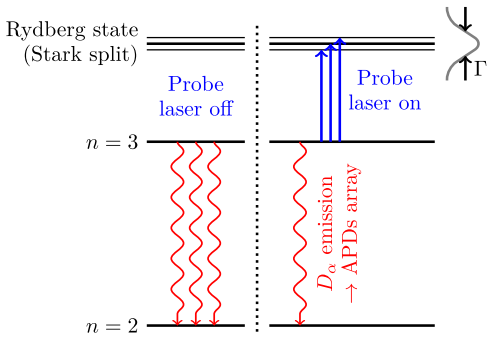

FIG. 1. Illustration of the LIRyS scheme. The left panel represents the D_α transition when the probe laser is OFF. The right panel illustrates the depopulation of the $n = 3$ level by resonant laser excitation of the atom to a Rydberg state resulting in a reduced D_α emission ($n = 3 \rightarrow 2$).

to depopulate the $n = 3$ level by exciting D atoms to a Rydberg state. Continuous tuning of the laser wavelength allows reconstructing the Rydberg level pattern characterized by the full width at half maximum (FWHM, Γ) of the corresponding transition. The key feature of the LIRyS approach is the wavelength resolved measurements of the D_α signal, which can directly be related to the electric field.

Figure 2 displays the calculated profiles of transitions from the $n = 3$ level to various Rydberg states as a function of the electric field's magnitude. Here, the gray bands represent the expected splitting [Eq. (1)] when Stark and Doppler broadenings[14,15] are not included. The transition's full line-widths are indicated using the red bands calculated for plasma density $n_e = 10^{13}$ cm^{-3} and temperature $T_e = 50$ eV. While higher Rydberg states ensure better sensitivity in measurements of the electric field $\mathcal{E}$, their mixing threshold is lower as can be derived from analyzing Fig. 2. Therefore to measure electric

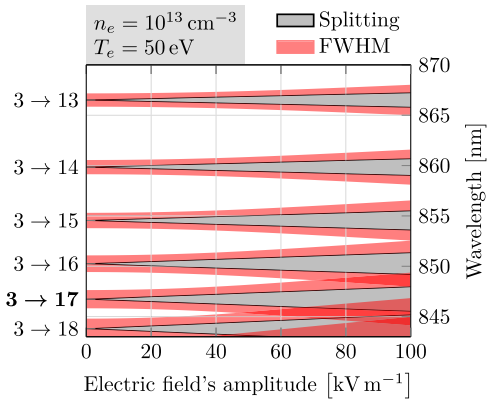

FIG. 2. Transition wavelengths and Stark splitting range. The broadening, half width at half maximum calculated from the computed spectrum (Fig. 3), is represented with the red zone. Interpolations have been used for values of the broadening on regions with overlapping states.

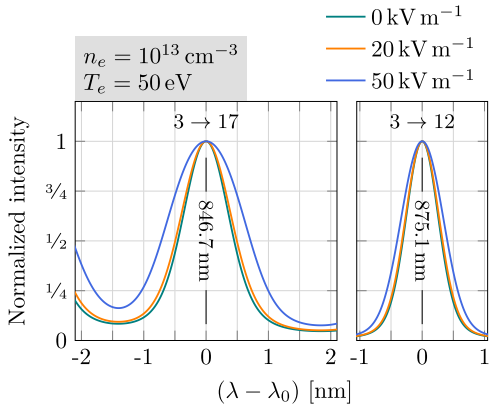

FIG. 3. Computed hydrogen spectrum for transitions from the level $n = 3$ to the 12th and 17th levels. This spectrum corresponds to the broadened profile from Stehlé and Hutcheon[16] database and calculated for three external electric field's amplitudes (0 kV m^{-1}, 20 kV m^{-1}, and 50 kV m^{-1}).

fields up to 50 kV m^{-1}, the 17th Rydberg level was selected (transition $n = 3 \rightarrow 17$).

The full transition broadenings in Figs. 2 and 3 are determined using the convolution of a thermal component (Gaussian) and a pressure component due to the presence of charged particles (Lorentzian) with the split energy levels. The values of each component are taken from the tabulated values available in Stehlé and Hutcheon[16] database. The resulting simulated linewidths are displayed in Fig. 3 for three different amplitudes of the electric field (0 kV m^{-1}, 20 kV m^{-1}, and 50 kV m^{-1}).

Figure 3 shows the spectrum for transitions to high n number states from the $n = 3$ level. The line-width changes substantially due to an external field. In our model, the full half-width Γ is assumed to be only function of the plasma parameters n_e, T_e, and $\mathcal{E}$, i.e., $\Gamma = \Gamma(\mathcal{E}, n_e, T_e)$. Given these dependencies, it is imperative to simultaneously determine the line-width of the transition to a Rydberg state and the plasma parameters (n_e, T_e). This is achieved with the LIRyS and the Thomson-scattering system probing the same observation volume (the intersection of the line of sight of the collection optics and the laser beam) as described below.

B. Implementation

To record the shape of the D_α emission's dip, a probe laser scans a resonant frequency $n = 3 \rightarrow$ Rydberg. To facilitate the sampling of the same collection volume as the Thomson-scattering, the probe laser is collinear

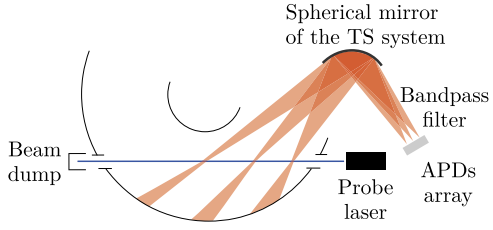

FIG. 4. Mid-plane top view representation of NSTX-U. The focus is made on the interaction volumes, i.e., interaction between the line of sight (in red) of each detectors and the probe laser (blue).

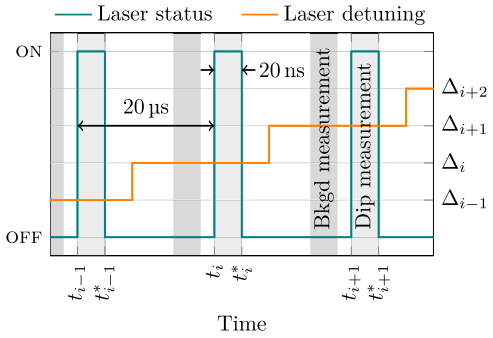

FIG. 5. Schematic description of the measurement process. Excitation laser (enabling the transition $3 \rightarrow 17$ to deplete the $n = 3$ level) is fired every 20 μs. The pulse width is 20 ns pulse. Each pulse is tuned at different wavelengths (indicated using Δ_j, $j = i - 1, i, \ldots$) around the resonance. The D_α photon-count is recorded before the laser pulse (background signal) and during laser duration for background subtraction.

to the Thomson-scattering laser system enabling measurements of the electron temperature and density at the same location as the depopulation-volume (see the schema in Fig. 4).

As the laser wavelength is tuned across the transition $n = 3 \rightarrow 17$, the D_α signal is recorded both during a laser pulse and in-between two laser pulses (for background reference) as illustrated in Fig. 5. In this figure, the signal acquisition time-windows are displayed in gray and light-gray for the background and dimmed-signal measurements, respectively. Note that temporal resolution of measurements is dictated by the sweeping rate of the laser cavity over the range of wavelengths of interest. Finally, the use of the existing Thomson-scattering system with high throughput would make the implementation of LIRyS straightforward at potentially reduced cost. Depending on the transition's linewidth, using commercially available components, we predict an achievable temporal resolution ranging from 2.5 ms to 10 ms.

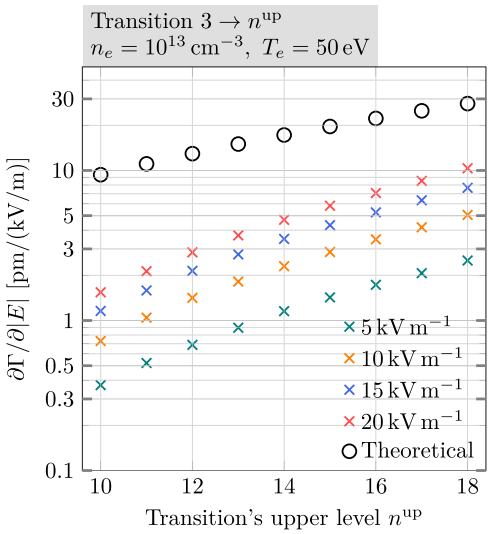

FIG. 6. Theoretical and true sensitivity of the width measurement to the external electric field. The theoretical sensitivity comes from the pure Stark splitting, whereas the true splitting includes the line-shape, varying according to the plasma parameters.

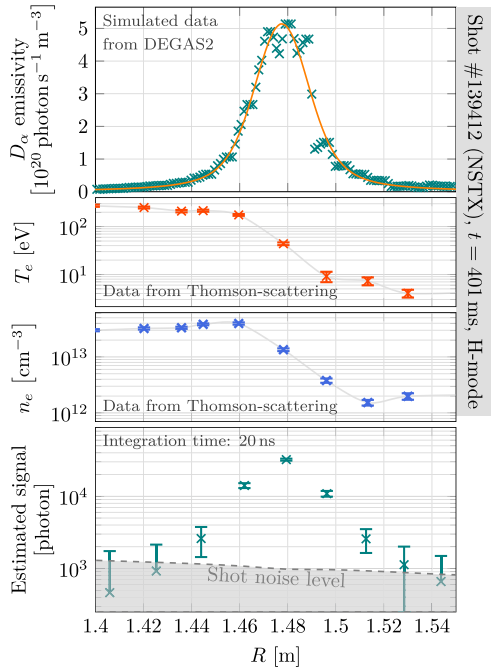

FIG. 7. Radial profile of the D_α emissivity issued by DEGAS2 simulations[21] (top), alongside with Thomson-scattering data for the plasma temperature and density (middle). At the bottom, the simulated signal difference acquired with and without the probe laser.

C. Sensitivity and dynamic range

The choice of the laser frequency and sweep range is dictated by the requested sensitivity and range of interest for the electric field to be measured. The sensitivity to the electric field varies significantly [see Eq. (1) and Fig. 2] between transitions, more specifically with the upper state of the transition.

We show in Fig. 6 the sensitivity of the full half-width as a function of the transition's upper level for a range of electric fields. In this figure, the black circles represent the maximum achievable sensitivity, which corresponds to an ideal case in the absence of any kind of broadening. With accounted broadenings, the sensitivity is reduced, especially at low amplitude of the external electric field. This trend remains true for any plasma parameters. However, as the broadening narrows (i.e., lower density and temperatures) the sensitivity can be greatly improved (see Sec. III).

As expected from Eq. (1) and shown in Fig. 6, one has to choose the largest upper state number available to maximize

TABLE II. Photon count and approximate Thomson-scattering parameters at different radii for a H-mode plasma (#139412 at t = 401 ms).

Radius (m)	Background[a] (Photon)	Signal[a] (Photon)	n_e (10^{12} cm^{-3})	T_e (eV)
1.44	335 826	2 599	37.8	215
1.46	303 002	14 102	37.1	160
1.47	272 452	32 194	12.4	40
1.49	244 140	10 875	3.7	9
1.51	218 120	2 575	1.5	7
1.52	194 459	1 128	1.9	4

[a]Integration time of 20 ns.

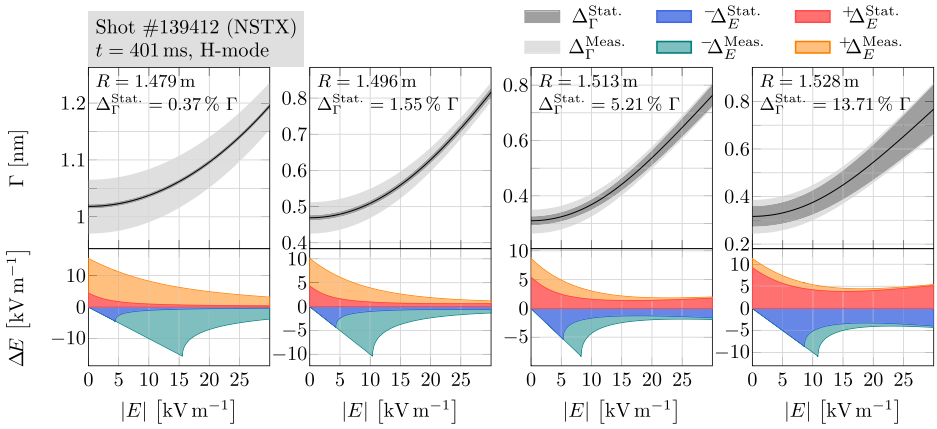

FIG. 8. Line-width dependency on the external electric field's amplitude at different positions in the plasma (top). The experimental and statistical uncertainties are represented with gray bands, respectively, due to Thomson-scattering error bars (on T_e and n_e) and to the fitting procedure. The latter is proportional to the signal to noise ratio (SNR) with a factor estimated through Monte-Carlo simulations. The associated uncertainty of the measurement of the electric field (bottom) is split into positive and negative components (asymmetrical) and detailed with respect to the source of the uncertainty (respectively, stat. or meas.).

the sensitivity—and therefore precision—for the LIRyS diagnostic. However, the energy states get denser as n^{up} increases which leads to a non-negligible mixing of the broadened states. The working range of the diagnostic is guided by the expected electric field's amplitude at the edge of a specific device. For instance, for the electric field weaker than 20 kV m^{-1} (as reported by Refs. 17–20), the transition $n = 3 \rightarrow 17$ is optimum in order to have sufficient margin in the dynamic range as well as a clear state separation.

In addition to the theoretical sensitivity of the LIRyS diagnostic, the uncertainty of the electron density and temperature (Thomson-scattering system) contributes to the electric field measurement errors. These variations have been analyzed using the data from Stehlé and Hutcheon[16] database; notably, Γ has a weak dependence on density variations for low densities which will then result in minimal impact in the electric field determination.

III. FORWARD MODELING

A. Signal estimation

With the probe laser ON, part of the D_α emission will be "switched OFF" equivalent to a drop in photon count for D_α. It is hence crucial to estimate this drop in photons.

We present the modeling and proof of principle for the implementation for such a diagnostic. One refers to the number of photons coming from the plasma in the absence of the probe laser as *background* and *signal* denoting the photon-count difference when the $n = 3$ level is half-depopulated in the collection volume. Note that this analysis is a geometric integration of the D_α emission.

The top panel of Fig. 7 represents the radial profile of the D_α emissivity. The emissivity was determined by simulations using the DEGAS2 code as reported by Stotler *et al.*[21] Given that the viewing chords are minimally changed in NSTX-U, this analysis also applies to NSTX-U. The two middle panels of Fig. 7 represent the electron density and temperature profiles. Finally, the bottom panel shows the estimated maximal number of photons to be observed. It is clear that the radial profile of the photon estimation tracks well the emissivity profile of D_α. In the shaded area, we indicate the shot noise level, calculated from the photon-counts based on Poisson statistics.

Table II summarizes the results of the geometrical integration of the D_α emissivity (Fig. 7) along the line of sight of each detector from the Thomson-scattering collection optics. It is worth noting that at sufficiently high (~150) laser energy the $n = 3$ level is depopulated by half in 0.5 ns ($\ll$20 ns). Therefore, the dip in D_α emission will remain constant during most of the 20 ns laser pulse.

B. Electric field determination

To demonstrate the capabilities of the proposed LIRyS diagnostic in measuring the electric field in NSTX (and NSTX-U), we performed synthetic diagnostics at four selected radial positions. Figure 8 displays the expected full half-width for electric fields ranging from 0 to 30 kV m^{-1} which is suitable for the selected 17th Rydberg level (transition $n = 3 \rightarrow 17$).

The probe laser sweep range is determined by the transition's full width at half maximum given by Γ. For example, the largest Γ (at the radial position $R = 1.47$ m) is about 1 nm. One can gain a factor two in the temporal resolution if one scans only half of the full-width. The experimental and statistical uncertainties are represented by shaded regions in Fig. 8 (both top and bottom panels). Moreover, we assume that the laser energy (E_L = ~150 μJ for the case discussed above) is sufficient to saturate the transition. Further discussions on the laser energy requirements can be found in Ref. 22.

IV. SUMMARY

We presented an approach that could provide direct measurements of the local electric field in the edge of tokamaks. The analysis, through forward modeling of the Stark spectra, shows that electric field precision of less than ±2 kV m^{-1} in regions with a local electric field of 15 kV m^{-1} can be achieved with a temporal resolution of 2.5 ms–10 ms. While this analysis was performed in H-mode plasmas, preliminary

analysis using NSTX-U L-mode plasmas has shown a factor two improvement in the electric field precision. Note that these values are determined when the local electron density and temperature are accurately known, which motivated the choice of having the LIRyS diagnostics collinear with the Thomson scattering system. Better resolution is achievable for low densities and low temperature plasma's regions, as Γ has a reduced sensitivity to experimental uncertainties. Furthermore, any improvement in the Thomson scattering system would be beneficial for the precision of LIRyS. Finally, we are evaluating other variations of LIRyS to make it self-calibrating. One such approach could be adapted to the tokamak and stellarator divertors where densities and temperatures are low. The subject of these approaches will be discussed in future work.

ACKNOWLEDGMENTS

The authors gratefully acknowledge discussions with R. E. Bell, B. P. LeBlanc, F. Scotti, and D. P. Stotler. The work was supported by U.S. Dept of Energy Contract No. DE-AC02-09CH11466 and based on L.R. Master's thesis. The digital data for this paper can be found following the links from http://arks.princeton.edu/ark:/88435/dsp01c247dv80k.

[1] A. Field, G. Fussmann, and J. Hofmann, Nucl. Fusion **32**, 1191 (1992).
[2] C. C. Klepper *et al.*, Rev. Sci. Instrum. **85**, 11E301 (2014).
[3] E. Trier *et al.*, Nucl. Fusion **48**, 092001 (2008).
[4] I. S. Bondarenko *et al.*, Rev. Sci. Instrum. **72**, 583 (2001).
[5] A. Fujisawa *et al.*, IEEE Trans. Plasma Sci. **22**, 395 (1994).
[6] B. W. Rice *et al.*, Phys. Rev. Lett. **79**, 2694 (1997).
[7] K. Ida, Plasma Phys. Controlled Fusion **40**, 1429 (1998).
[8] A. J. H. Donné, Plasma Phys. Controlled Fusion **44**, B137 (2002).
[9] I. V. Hertel and C.-P. Schulz, *Atoms, Molecules and Optical Physics 1*, Graduate Texts in Physics (Springer, Berlin, 2015).
[10] W.-y. Tsai, Phys. Rev. A **9**, 1081 (1974).
[11] *Springer Handbook of Atomic, Molecular, and Optical Physics*, edited by G. Drake (Springer, New York, 2006).
[12] A. Osterwalder and F. Merkt, Phys. Rev. Lett. **82**, 1831 (1999).
[13] U. Czarnetzki, D. Luggenhölscher, and H. F. Döbele, Phys. Rev. Lett. **81**, 4592 (1998).
[14] H. R. Griem, *Spectral Line Broadening by Plasmas*, Pure and Applied Physics Vol. 39 (Academic Press, New York, 1974).
[15] H.-J. Kunze, *Introduction to Plasma Spectroscopy*, Springer Series on Atomic, Optical, and Plasma Physics Vol. 56 (Springer, Berlin, 2009).
[16] C. Stehlé and R. Hutcheon, Astron. Astrophys., Suppl. Ser. **140**, 93 (1999).
[17] M. Cavedon *et al.*, Plasma Phys. Controlled Fusion **59**, 105007 (2017).
[18] A. Diallo *et al.*, Nucl. Fusion **53**, 093026 (2013).
[19] J. Hillesheim *et al.*, Phys. Rev. Lett. **116**, 065002 (2016).
[20] L. Krupnik *et al.*, Czech. J. Phys. **55**, 317 (2005).
[21] D. P. Stotler *et al.*, Phys. Plasmas **22**, 082506 (2015).
[22] L. Reymond, "Forward modeling for the development of a laser-induced Rydberg spectroscopy diagnostic on NSTX-U," M.Sc. thesis, Ecole Polytechnique Fédérale de Lausanne, 2017.